Atmos. Chem. Phys., 8, 5529–5534, 2008
www.atmos-chem-phys.net/8/5529/2008/

Atmospheric Chemistry and Physics

Odin/OSIRIS observations of stratospheric NO_3 through sunrise and sunset

C. A. McLinden[1] **and C. S. Haley**[2]

[1]Environment Canada, Toronto, ON, M3H 5T4, Canada
[2]Centre for Research in Earth and Space Science, York University, Toronto, ON, M3J 1P3, Canada

Received: 17 January 2008 – Published in Atmos. Chem. Phys. Discuss.: 20 March 2008
Revised: 8 July 2008 – Accepted: 14 August 2008 – Published: 15 September 2008

Abstract. The nitrate radical (NO_3) has been detected in visible limb-scattered spectra measured by the Optical Spectrograph and InfraRed Imager System (OSIRIS) onboard the Odin satellite when observing at large solar zenith angles (91–97°). Apparent slant column densities of NO_3 at tangent heights between 10 and 45 km are derived via spectral fitting in the 610–680 nm window. Using observations from multiple scans spanning solar zenith angles of 91–97°, the rapid evolution of NO_3 through sunrise and sunset can be traced. Slant column densities are found to be generally consistent with those simulated using a radiative transfer model with coupled photochemistry. In addition, a strong dependence of NO_3 with temperature is observed. These results indicate that our current knowledge of NO_3 photochemistry is generally consistent with OSIRIS observations to within the limitations of the radiative transfer modeling. Furthermore, they reveal that OSIRIS possesses signal-to-noise sufficient to make useful measurements of scattered sunlight out to solar zenith angles of 91–97° and suggest the possibility of retrieving profile information for NO_3 and other species at large solar zenith angles.

1 Introduction

An important player in nighttime stratospheric photochemistry is the nitrate radical, NO_3. In the absence of sunlight, the following Reactions (R1)–(R3) largely govern the stratospheric NO_3 abundance:

$$O_3 + NO_2 \rightarrow O_2 + NO_3 \quad \text{(R1)}$$

$$NO_3 + NO_2 + M \rightarrow N_2O_5 + M \quad \text{(R2)}$$

$$N_2O_5 + M \leftrightarrow NO_3 + NO_2 + M \quad \text{(R3)}$$

Since N_2O_5 may be converted to HNO_3 on the surface of aerosols, NO_3 represents a key intermediary in the conversion of NO_y from an active (NO and NO_2) to an inactive (HNO_3) form. At solar zenith angles (SZAs) less than about 93–96°, which corresponds to sunset/sunrise in the stratosphere, photolysis rapidly destroys NO_3, thereby suppressing its abundance to a small fraction of its nighttime values. To date all successful measurements of stratospheric NO_3 have been made by measuring light which has sampled the atmosphere at SZA$\gtrsim$93° (the SZA at the observation point is smaller, but a portion of its path has traversed larger SZAs). Figure 1 illustrates the evolution of NO_3 profiles calculated using the University of California, Irvine (UCI) photochemical box model (Prather, 1992; McLinden et al., 2000) through sunrise and sunset. It shows the NO_3 number density as a function of altitude at several SZAs, including 100° which was chosen to represent nighttime. The months and latitudes were chosen to be representative of the location of the observations shown below. Note that refraction is not included in the UCI model. At the onset of sunrise (panel a) at the top of the stratosphere (50 km altitude, SZA$\backsimeq$97°) NO_3 remains at its nighttime value until there is direct illumination of the upper stratosphere. At a SZA of 96°, NO_3 below ~30 km remains near its maximum while above this altitude there is substantial destruction from photolysis. At a SZA of 93°, NO_3 is reduced by more than an order of

Correspondence to: C. A. McLinden
(chris.mclinden@ec.gc.ca)

Published by Copernicus Publications on behalf of the European Geosciences Union.

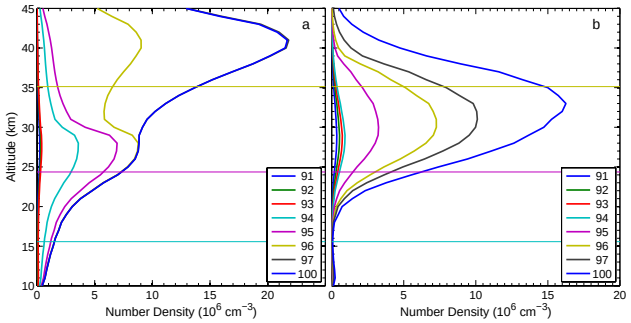

Fig. 1. Diurnal variation of NO_3 as calculated in the photochemical box model at several solar zenith angles: **(a)** sunrise on 15 December at 35° N and **(b)** sunset on 15 June at 0° N. The horizontal lines indicate the altitude of Earth's shadow in the photochemical model, colour-coded according to the solar zenith angle. In panel **(a)** the 97 and 100° traces are virutally identical.

magnitude as the entire stratosphere is now directly illuminated. The growth of NO_3 begins as the sun sets (panel b) in the stratosphere but is delayed (relative to sunrise) due to the time constant of Reaction (R1), about 5 min at 40 km. While the local time difference (sunrise vs. sunset) drives most of the differences in these two panels, the difference in latitude and time-of-year also plays a role directly via the NO_y profile and through the rates of Reactions (R1)–(R3) via ozone and temperature profiles. As a rough approximation, different seasons and latitudes may modify the values in each panel by a factor of two but the character of the SZA-dependence remains the same.

Historically, ground-based lunar measurements (e.g., Noxon et al., 1978; Smith and Solomon, 1990; Wagner et al., 2000) have been used most extensively to measure NO_3. Stellar and lunar occultation of NO_3 has also been successful in retrieving NO_3 profiles (Renard et al., 2001, 2005), most recently with the SCIAMACHY (SCanning Imaging Absorption SpectroMeter for Atmospheric CHartographY) (Amekudzi et al., 2005), SAGE (Stratospheric Aerosol and Gas Experiment) III (R. Moore, 2006, personal communication), and GOMOS (Global Ozone Measured by Occultation of Stars) (Marchand et al., 2004) satellite instruments. Lunar and stellar systems are advantageous since their light source is dim enough to not affect the NO_3 abundance. Other ground-based systems, such as zenith-sky spectroscopy (Coe et al., 2002) and the off-axis technique (e.g., Weaver, 1996), employ the Sun as a source and observe during twilight. The key with all methods that measure Sunlight is to observe light that has traversed a range of SZAs in order to both have a large enough photon signal to overcome noise but also to sample local night where NO_3 is abundant. All told there have been relatively few measurements of stratospheric NO_3 made to date with only GOMOS providing large-scale, vertically-resolved coverage (Marchand et al., 2004).

This work examines the utility of OSIRIS (Optical Spectrograph and InfraRed Imager System) for sensing stratospheric NO_3. OSIRIS, in orbit on the Odin satellite since 2001, measures sunlight scattered from the Earth's limb from 7–70 km in tangent height and between 280 and 800 nm at ∼1 nm resolution (Llewellyn et al., 2004). While a limb-scatter instrument is not an obvious candidate for NO_3 retrievals, Odin resides in a Sun-synchronous, near-terminator orbit. This means OSIRIS, which was designed for observing at low light levels, generally observes near sunrise and sunset.

2 OSIRIS observations of NO_3 apparent slant column densities

For optimal NO_3 detection, OSIRIS needs to look as far off the terminator as possible in order to maximize the variation of the SZA along the line-of-sight (LOS). Additionally, the scattering angle (or, the angle between the incoming sunlight and the OSIRIS LOS) must be a minimum so that OSIRIS is on the night side of the tangent point. This geometry increases the photon signal due to the (relatively) small SZAs at the tangent point, and also increases the NO_3 absorption signal as this light must traverse larger SZAs, and hence NO_3 abundances, on its way to OSIRIS. Using these criteria the optimal period to observe NO_3 at sunrise is in December on the descending node (scattering angle of ∼74°) and NO_3 at sunset is in June on the ascending node (scattering angle of ∼58°). This study will focus exclusively on these periods. The amount by which the SZA varies along the LOS depends heavily on the particular geometry, but representative numbers are 3° for the sunrise period and 2° for the sunset period (McLinden et al., 2006). These numbers represent the change in SZA between the tangent point and one scale height above the tangent point (along the LOS).

The spectral fitting routine of Haley et al. (2004) was used to derive apparent slant column densities (SCDs) of NO_3 between 10 and 45 km. The SCD represents the number density weighted by the pathlength of the scattered sunlight through the atmosphere. Possible paths include single-scattered, multiple-scattered, as well as light reflected from the surface into the observing LOS. Considering the utilized wavelengths (see below) and large SZAs, a large fraction of the detected light originates from singly-scattered photons. The fitting window 610–680 nm was selected over the more common 640–680 nm window as it contains two large NO_3 features (instead of one) and provides increased signal-to-noise (due to more pixels) and reduced correlations with other absorbers, particularly ozone. The two spectral windows give very similar SCDs. For each scan the reference spectrum was obtained by co-adding all spectra from that scan with tangent heights between 45 and 55 km. The NO_3 cross-sections

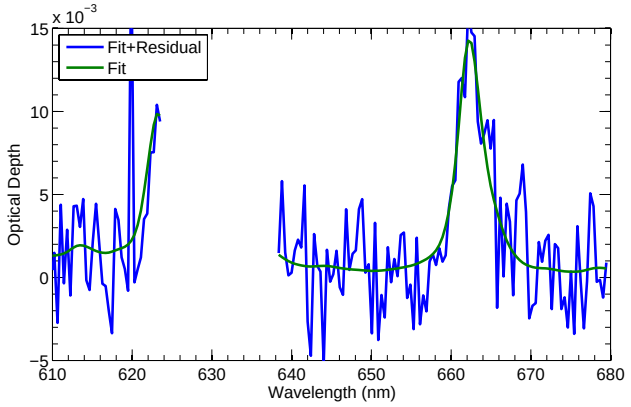

Fig. 2. Results of a typical spectral fit. Shown are the fitted NO_3 optical depth spectrum and the fitted NO_3 plus the residual of the fit for scan 15 179 021 (7 December 2003; tangent height=39 km; latitude=40° N; longitude=47° E; SZA=95.4°). The fitted NO_3 SCD is 7.2×10^{14} cm^{-2} and the RMS-residual (over wavelength) is 0.0027. The region near 630 nm is not included in the fit (see text).

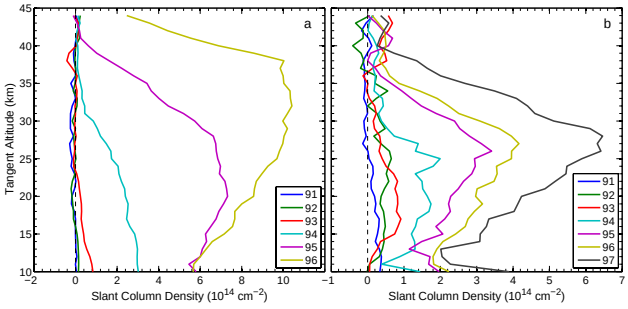

Fig. 3. Mean OSIRIS NO_3 apparent slant column densities as a function of tangent altitude for **(a)** sunrise over 1–21 December 2003 (20–45° N) and **(b)** sunset over 6 June–3 July 2004 (5° S–10° N).

at 298 K are scaled to a temperature of 230 K (Orphal et al., 2003). Other species included in the spectral fit are ozone (221 K) (Bogumil et al., 2003), NO_2 (202 K) (Vandaele et al., 1998), O_4 (Belgian Institute for Space Aeronomy, http://www.aeronomie.be/spectrolab/o2.htm), and H_2O (see below). Rayleigh, tilt/undersampling (Sioris et al., 2003) and polarization (McLinden et al., 2002b) pseudo-absorbers were also included. A second-order closure polynomial was used and no correction for the Ring effect was performed as it has only a small effect in this region.

Water vapour cross-sections at 10 hPa and 243 K were derived using line parameters from HITRAN 2003 in a line-by-line code (Y. Rochon, personal communication) and smoothed to the resolution of OSIRIS. It was found that including additional H_2O cross-sections at other pressures and temperatures, or a pseudo-absorber for the H_2O temperature dependence (Aliwell and Jones, 1996), had little impact and so were not included. This is likely due to a very small contribution from multiple-scattered and surface-reflected light that has sampled the water-rich troposphere.

A representative spectral fit is shown in Fig. 2. The two largest NO_3 absorption features at 623 and 662 nm are clear. Based on the fitting residuals it is estimated that the detection limit is $<5\times10^{13}$ cm^{-2} for SZAs of 95° and smaller and 1×10^{14} cm^{-2} for larger SZAs. A section of the spectra near 630 nm was excluded from the fit since it contains a combination of the red-line of atomic oxygen and the O_2–γ band, complex spectral features not easily accounted for in the fitting procedure.

In this study two periods of OSIRIS data were analyzed: (i) 1–21 December 2003 covering 94 orbits and (ii) 6 June–3 July 2004 covering 150 orbits. Sunrise in the December period covered a latitude band between 20° N to 45° N with a total of 380 scans, about 3–6 scans per orbit. Sunset in June occurred over the equator (5° S to 10° N) with 115 total scans, 2–4 per orbit. The June data is sparser due to OSIRIS observing in so-called "strat-meso" mode in which limb scans extended up to 110 km (as opposed to the typical 70 km). All NO_3 SCDs were interpolated onto a standard tangent height grid and grouped into 1° SZA bins between 91° and 97° using the SZA at the tangent point. Due to the rapid variation of NO_3 with SZA, and recognizing that SZA changes by 0.5° to 0.8° over the course of a scan, each tangent height observation was sorted according to its particular SZA (as opposed to the representative SZA assigned to the entire scan). Thus, observations from a given scan often span two SZA bins. Only scans in which the minimum in radiance signal-to-noise ratio between 10–45 km in the fitting window exceeded 10 were processed.

The mean NO_3 SCDs in each bin are shown in Fig. 3 during sunrise and sunset. At a SZA of 96° during sunrise NO_3 abundances are near their night-time levels but once the sun rises, initially in the upper stratosphere, there is rapid destruction via photolysis. This destruction progresses downward as the sun rises further. At a SZA of 93° there is only a small amount of NO_3 remaining near 12 km and at a SZA of 92° the SCDs do not differ significantly from zero. During sunset there is essentially no NO_3 until a SZA of 94°, where it begins to form after the sun has set in the lower stratosphere. The peak SCD in the sunset data occurs lower than for sunrise, consistent with the model results in Fig. 1. At sunrise there is insufficient signal to obtain SCDs at a SZA of 97°. Due to the different scattering angles between sunrise and sunset there is a factor of 3–5 smaller signal during sunrise as compared to sunset at a SZA of 97°.

Note that significant SCDs exist at tangent heights in which the Sun is below the local horizon. For example, at 22 km sunset/sunrise occurs at a SZA of about 95°.

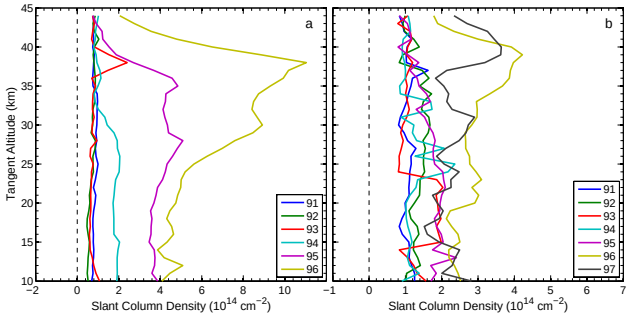

Fig. 4. Standard deviations of OSIRIS NO_3 apparent slant column densities as a function of tangent altitude for **(a)** sunrise over 1–21 December 2003 (20–45° N) and **(b)** sunset over 6 June–3 July 2004 (5° S–10° N).

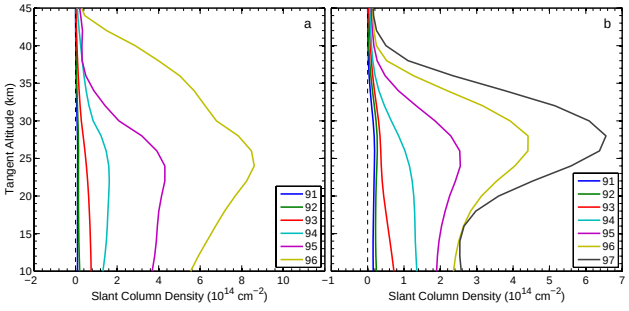

Fig. 5. Modelled NO_3 apparent slant column densities as a function of tangent altitude for **(a)** sunrise on 15 December (35° N) and **(b)** sunset on 15 June (0° N). The scale has been chosen to match that in Fig. 3.

This absorption signal arises from light scattered into the LOS on the far side of the tangent point where the SZAs are smaller (and hence experience direct illumination) that then traverses the NO_3-abundant air on the near side of the tangent point. It is the range of SZAs along a LOS that effectively smoothes the variation of SCD with tangent height, even when the local terminator is crossed.

The standard deviations (STDs) about the NO_3 SCD means are shown in Fig. 4. The sunrise STDs (panel a) are found to increase with SZA (and mean SCD). The primary reason for these large values is believed to be the temperature dependence of Reactions (R1) and (R3). Differences in temperature at the different scan locations lead a large separation in the NO_3 abundances throughout the night. This is discussed further below. The sunset STDs (panel b) are smaller and vary less with SZA although they are still a substantial fraction of the mean SCDs. Considering this large source of natural variability it is concluded that the STD is not a good measure of the precision of an individual SCD profile.

3 Modelling of NO_3 slant column densities

While the observations presented in Fig. 3 appear to be qualitatively consistent with our knowledge of NO_3, the question remains: are they quantitatively consistent? To address this, NO_3 SCDs are forward-modelled using the VECTOR (Vector Order-of-scattering Radiative Transfer) model (McLinden et al., 2002a, 2006). VECTOR is coupled to the UCI photochemical box model and takes into account the so-called diurnal effect (or, the variation of a diurnally varying species such as NO_3 along the LOS with SZA) (McLinden et al., 2006). The box model used a climatological atmosphere for the specified month and latitude (McLinden et al., 2000) and reaction rate data from the JPL 2006 compendium (Sander et al., 2006). In order to adequately capture the rapid variation of NO_3 with SZA the vertical grid in VECTOR was set to 0.5 km. Spectra were generated at 0.1 nm resolution, smoothed to OSIRIS resolution, and then a spectral fit was applied, analogous to the analysis of the OSIRIS spectra. In this way representative synthetic SCDs are generated for the two periods: 15 December, 35° N at sunrise and 15 June, 0° N at sunset. Each set of calculations was performed using the mean scattering angle (or, angle between the incoming solar beam and the observing LOS) for that period and latitude and over a range of SZAs. Note that neither VECTOR nor the photochemical box model account for refraction.

Results from the NO_3 SCD simulations are presented in Fig. 5 for sunrise and sunset and are analogous to the observations plotted in Fig. 3. In general the simulated values are similar to the observations. However, there appear to be some differences in the decay of NO_3 after sunrise, with the modeled SCDs leading the observations by about 0–0.5° with the largest differences in the upper stratosphere. The modeled sunset and observed SCDs are found to be very similar at the larger SZAs, 96–97°, but at 94–95° the model calculations seem to be leading the observations. Possible reasons for these inconsistencies include neglecting refraction in the model, an inconsistent atmosphere (particularly ozone and temperature), or erroneous rate constants. Considering these caveats, the magnitude and behaviour with SZA appear generally consistent between the modeled and observed SCDs. Additional work, including the incorporation of refraction into the models, is required to better understand these differences.

4 Case study: successive orbits on 7 December 2003

Scans from successive orbits on 7 December 2003 are examined in greater detail. The NO_3 SCDs from these orbits are found to differ dramatically, sometimes by a factor of 3 or more. Two scans, one from each orbit, are shown in Fig. 6 (panel a) along with their uncertainties. Note the uncertainty,

as determined from the spectral fitting, is $\sim 1 \times 10^{14}$ cm^{-2} and is much smaller than the signals. These two scans were taken at nearly identical latitudes (40° N) and SZAs (95.5°) and separated in longitude by 24°. Scan 1 (orbit 15 179, scan 021) SCDs are $\sim 10 \times 10^{14}$ cm^{-2} larger than scan 2 (orbit 15 180, scan 021) below 35 km, but are smaller above 38 km. The primary cause of this is thought to be the difference in local temperature at the location of each scan. The temperature difference, from ECMWF reanalysis data, is shown in Fig. 6 (panel b) where, between 30 and 40 km, scan 1 temperatures are warmer above 25 km, with the temperature difference reaching a maximum of 20 K at 35 km. Reactions (R1) and (R3) are very temperature dependent, with warmer temperature favouring increased NO_3, and a 15 K increase in temperature amounts to a factor of ∼2 increase in the rate coefficient for reaction (R1) (Sander et al., 2006). The tangent height at which scan 1 becomes larger than scan 2, ∼38 km, can be compared to the altitude at which the temperature (at the tangent point) of scan 1 becomes larger, ∼42 km. Considering that temperature is a local quantity while SCDs are non-local, the SCDs appear at least qualitatively consistent with the temperature profiles. Likely adding to the differences are the ∼20% larger ozone SCDs in scan 1 (not shown) via Reaction (R1). The fact that the difference in SCD remains constant into the lower stratosphere reflects the fact that much of the absorption occurs in the upper stratosphere even at lower tangent heights. Above 42 km scan 1 is colder, roughly corresponding to the the altitudes where scan 1 displays smaller SCDs.

To add support to the assertion that the temperature differences are primarily responsible for the difference in SCDs, box model simulations were carried out using the ECMWF temperature profiles from the locations of these scans with all other input parameters identical. The resultant NO_3 number density profiles are shown in Fig. 6 (panel c). Densities using the temperature for scan 1 are 3–4 times larger at 35 km, suggesting the larger SCDs are indeed feasible.

The relatively small uncertainties and the overall consistent picture from these scans suggest that individual scans possess sufficient signal-to-noise to derive NO_3 SCDs and that co-adding of spectra is not necessary.

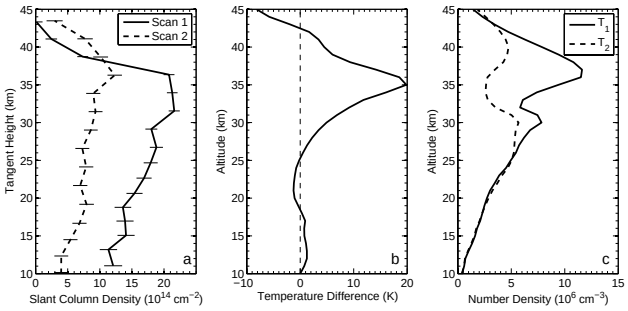

Fig. 6. Comparison of two scans for consecutive orbits on 7 December 2003 (scan 1: scan 15 179 021 at latitude 39.9° N and SZA of 95.5°; scan 2: scan 15 180 021 at latitude 40.0° N and SZA of 95.6°): **(a)** NO_3 slant column densities, including their uncertainty from the spectral fit, **(b)** the difference between the scan 1 and scan 2 ECMWF temperature profiles, T(scan 1)–T(scan 2), **(c)** box model simulations of NO_3 for 7 December at 40° N and a SZA of 95.5° initialized using scan 1 (T_1) and scan 2 (T_2) temperature profiles.

5 Conclusions

The nitrate radical (NO_3) has been detected in visible limb-scattered spectra measured by the Optical Spectrograph and InfraRed Imager System (OSIRIS) on-board the Odin satellite when observing through sunrise and sunset in the stratosphere. Apparent slant column densities (SCDs) of NO_3 as a function of tangent height are derived via spectral fitting in the 610–680 nm window. Using observations from multiple scans spanning SZAs of 91–97° the rapid evolution of NO_3 through sunrise and sunset can be traced. The derived SCDs are consistent with those simulated using a radiative transfer model with coupled photochemistry. A case study comparing two SCD profiles shows the important role temperature plays in the abundance of NO_3. The results indicate that our current knowledge of NO_3 photochemistry is generally consistent with OSIRIS observations to within the limitations of the radiative transfer modeling. Further, they show that OSIRIS possesses signal-to-noise sufficient to make useful measurements of scattered sunlight out to SZAs of 96–97° and furthermore suggests the possibility of retrieving vertical profiles of NO_3 number density and other absorbers (such as NO_2) at these large SZAs.

Logical next steps in the analysis of these data is to attempt the retrieval of profiles and to test the consistency of OSIRIS NO_3 by finding coincidences with SCIAMACHY, GOMOS, and/or SAGE III occultation measurements. The primary obstacle in either approach lies in the steep diurnal gradients along the LOS. As there is only enough information in a limb scan to retrieve a single profile (i.e. at one SZA), a photochemical model is required to map the NO_3 from the SZA at the tangent point to all other SZAs along the LOS.

Acknowledgements. The authors acknowledge the comments and insight of C. Sioris and the two anonymous referees. Odin is a Swedish-led satellite project funded jointly by Sweden (SNSB), Canada (CSA), France (CNES) and Finland (Tekes). Odin is also partially funded as an European Space Agency Third Party Mission.

Edited by: A. Richter

References

Aliwell, S. R. and Jones, R. L.: Measurement of atmospheric NO_3 1. Improved removal of water vapour absorption features in the analysis for NO_3, Geophys. Res. Lett., 23(19), 2585–2588, 1996.

Amekudzi, L. K., Sinnhuber, B.-M., Sheode, N. V., Meyer, J., Rozanov, A., Lamsal, L. N., Bovensmann, H., and Burrows, J. P.: Retrieval of stratospheric NO_3 vertical profiles from SCIAMACHY lunar occultation measurement over the Antarctic, J. Geophys. Res., 110, D20304, doi:10.1029/2004JD005748, 2005.

Bogumil, K., Orphal, J., Homann, T., Voigt, S., Spietz, P., Fleischmann, O. C., Vogel, A., Hartmann, M., Kromminga, H., Bovensmann, H., Frerick, J., and Burrows, J. P.: Measurements of molecular absorption spectra with the SCIAMACHY preflight model: Instrument characterization and reference data for atmospheric remote-sensing in the 230–2380 nm region, J. Photoch.. Photobio. A., 157(2–3), 167–184, 2003.

Coe, H., Allan, B. J., and Plane, J. M. C.: Retrieval of vertical profiles of NO_3 from zenith sky measurements using an optimal estimation method, J. Geophys. Res., 107(D21), 4587, doi:10.1029/2002JD002111, 2002.

Haley, C. S., Brohede, S. M., Sioris, C. E., Griffioen, E., Murtagh, D. P., McDade, I. C., Eriksson, P., Llewellyn, E. J., Bazureau, A., and Goutail, F.: Retrieval of stratospheric O_3 and NO_2 profiles from Odin/OSIRIS limb-scattered sunlight measurements, J. Geophys. Res., 109, D16303, doi:10.1029/2004JD004588, 2004.

Llewellyn, E. J., Lloyd, N. D., Degenstein, D. A., Gattinger, R. L., Petelina, S. V., Bourassa, A. E., Wiensz, J. T., Ivanov, E. V., McDade, I. C., Solheim, B. H., McConnell, J. C., Haley, C. S., von Savigny, C., Sioris, C. E., McLinden, C. A., Griffioen, E., Kaminski, J., Evans, W. F. J., Puckrin, E., Strong, K., Wehrle, V., Hum, R. H., Kendall, D. J. W., Matsushita, J., Murtagh, D. P., Brohede, S., Stegman, J., Witt, G., Barnes, G., Payne, W. F., Piché, L., Smith, K., Warshaw, G., Deslauniers, D.-L., Marchand, P., Richardson, E. H., King, R. A., Wevers, I., McCreath, W., Kyrölä, E., Oikarinen, L., Leppelmeier, G. W., Auvinen, H., Mégie, G., Hauchecorne, A., Lefèvre, F., de La Nöe, J., Ricaud, P., Frisk, U., Sjoberg, F., von Schéele, F., and Nordh, L.: The OSIRIS instrument on the Odin satellite, Can. J. Phys., 82(6), 411–422, 2004.

Marchand, M., Bekki, S., Hauchecorne, A., and Bertaux, J. L.: Validation of the self consistency of GOMOS NO_3, NO_2 and O_3 data using chemical data assimilation, Geophys. Res. Lett., 31, L10107, doi:10.1029/2004GL019631, 2004.

Marchand, M., Bekki, S., and Hauchecorne, A.: Temperature retrieval from stratospheric O_3 and NO_3 GOMOS data, Geophys. Res. Lett., 34, L24809, doi:10.1029/2007GL030280, 2007.

McLinden, C. A., Olsen, S. C., Hannegan, B., Wild, O., Prather, M. J., and Sundet, J.: Stratospheric ozone in 3-D models: A simple chemistry and the cross-tropopause flux, J. Geophys. Res., 105(D11), 14 653–14 665, 2000.

McLinden, C. A., McConnell, J. C., Griffioen, E., and McElroy, C. T.: A vector radiative transfer model for the Odin/OSIRIS project, Can. J. Phys., 80(4), 375–393, doi:10.1139/p01-156, 2002a.

McLinden, C. A., McConnell, J. C., Strong, K., McDade, I. C., Gattinger, R. L., King, R., Solheim, B., Llewellyn, E. J., and Evans, W. F. J.: The impact of the OSIRIS grating efficiency on total radiance and trace-gas retrievals, Can. J. Phys., 80(4), 469–481, 2002b.

McLinden, C. A., Haley, C. S., and Sioris, C. E.: Diurnal effects in limb scatter observations, J. Geophys. Res., 111, D14302, doi:10.1029/2005JD006628, 2006.

Noxon, J. F., Norton, R. B., and Henderson, W. R.: Observation of atmospheric NO_3, Geophys. Res. Lett., 5(8), 675–678, 1978.

Orphal, J., Fellows, C. E., and Flaud, P.-M.: The visible absorption spectrum of NO_3 measured by high-resolution Fourier transform spectroscopy, J. Geophys. Res., 108(D3), 4077, doi:10.1029/2002JD002489, 2003.

Prather, M.: Catastrophic loss of stratospheric ozone in dense volcanic clouds, J. Geophys. Res., 97(D9), 10 187–10 191, 1992.

Renard, J.-B., Taupin, F. G., Rivière, E. D., Pirre, M., Huret, N., Berthet, G., Robert, C., Chartier, M., Pepe, F., and George, M.: Measurements and simulation of stratospheric NO_3 at mid and high latitudes in the Northern Hemisphere, J. Geophys. Res., 106(D3), 32 387–32 400, 2001.

Renard, J.-B., Chipperfield, M. P., Berthet, G., Goffinont-Taupin, F., Robert, C., Chartier, M., Roscoe, H., Feng, W., Rivière, E., and Pirre, M.: NO_3 vertical profile measurements from remote sensing balloon-borne spectrometers and comparison with model calculations, J. Atmos. Chem., 51, 65–78, 2005.

Sander, S. P., Friedl, R. R., Ravishankara, A. R., Golden, D. M., Kolb, C. E., Kurylo, M. J., Molina, M. J., Moortgat, G. K., Keller-Rudek, H., Finlayson-Pitts, B. J., Wine, P. H., Huie, R. E., and Orkin, V. L.: JPL 2006: Chemical kinetics and photochemical data for use in atmospheric studies - Evaluation 15, Jet Propul. Lab., Pasadena, Calif., JPL Publ. 06-2, 2006.

Sioris, C. E., Haley, C. S., McLinden, C. A., von Savigny, C., McDade, I. C., McConnell, J. C., Evans, W. F. J., Lloyd, N. D., Llewellyn, E. J., Chance, K. V., Kurosu, T. P., Murtagh, D. P., Frisk, U., Pfeilsticker, K., Bösch, H., Weidner, F., Strong, K., Stegman, J., and Mégie, G.: Stratospheric profiles of nitrogen dioxide observed by Optical Spectrograph and Infrared Imager System on the Odin satellite, J. Geophys. Res., 108(D7), 4215, doi:10.1029/2002JD002672, 2003.

Smith, J. P. and Solomon, S.: Atmospheric NO_3 3. Sunrise Disappearance and the Stratospheric Profile, J. Geophys. Res., 95(D9), 13819, 1990.

Vandaele, A., Hermans, C., Simon, P. C., Carleer, M., Colin, R., Fally, S., Mérienne, M. F., Jenouvrier, A., and Coquart, B.: Measurements of the NO_2 absorption cross-section from 42 000 cm^{-1} to 10 000 cm^{-1} (238–1000 nm) at 220 K and 294 K, J. Quant. Spectrosc. Ra., 59(3–5), 171–184, 1998.

Wagner, T., Otten, C., Pfeilsticker, K., Pundt, I., and Platt, U.: DOAS moonlight observation of atmospheric NO_3 in the Arctic winter, Geophys. Res. Lett., 27(21), 3441–3444, 2000.

Weaver, A.: Atmospheric NO_3 5. Off-axis measurements at sunrise: Estimates of tropospheric NO_3 at 40° N, J. Geophys. Res., 101(D13), 18 605–18 612, 1996.